NACA

RESEARCH MEMORANDUM

SOME EXPERIMENTAL EFFECTS OF AFTERBODY SHAPE ON THE ZERO-LIFT DRAG OF BODIES FOR MACH NUMBERS BETWEEN 0.8 AND 1.3

By William E. Stoney, Jr.

Langley Aeronautical Laboratory
Langley Field, Va.

NATIONAL ADVISORY COMMITTEE
FOR AERONAUTICS

WASHINGTON

October 1, 1953

CLASSIFICATION CANCELLED OR CHANGED TO Unclassified

BY AUTHORITY OF NASA Tech Ltr Announcement #120

(OFFICER AUTHORIZED TO CHANGE)

By 30 Oct 61

(GRADE OF OFFICER MAKING CHANGE)

30 Nov 61

DATE

NATIONAL ADVISORY COMMITTEE FOR AERONAUTICS

RESEARCH MEMORANDUM

SOME EXPERIMENTAL EFFECTS OF AFTERBODY SHAPE ON THE ZERO-LIFT DRAG OF BODIES FOR MACH NUMBERS BETWEEN 0.8 AND 1.3

By William E. Stoney, Jr.

SUMMARY

Zero-lift drag data were obtained on a series of fin-stabilized bodies differing only in afterbody shape. Three series of afterbodies (fineness ratios 1.78, 3.00, and 5) with varying ratios of base radius to maximum radius (0, 0.438, 0.700, and 1) were combined with a fineness-ratio-7.13 parabolic nose. Both conical and parabolic afterbodies were tested. The models were launched from the Langley helium gun at the testing station at Wallops Island, Va., and data were obtained for Mach numbers from 0.8 to 1.3, and for Reynolds numbers (based on body length) of about 10×10^6.

The results indicated that at supersonic speeds, linear theory in conjunction with estimated base pressures and fin drag was adequate to define the minimum-drag configurations (for given frontal area and fineness ratio) and gave fair predictions of the drag for all afterbodies of fineness ratios 3.50 and 5.00. The fineness-ratio-1.78 conical afterbodies showed appreciably lower drags than their parabolic counterparts; however, there was no difference between the two shapes for the fineness-ratio-5 afterbodies. From the test results, the following would appear to be useful criteria for the design of afterbodies having no issuing jet: A conical afterbody angle of about 4.5° will give the minimum drag for any fineness ratio less than 6. This angle may vary between 3.5° and 6.5° for configurations whose drag will be within 10 percent of the minimum. The minimum-drag afterbody is that of a fineness ratio of about 6 and its drag will be approximately 30 to 40 percent of that for a square-base body of fineness ratio 0.

INTRODUCTION

The problem of designing afterbody shapes for minimum drag at supersonic speeds is a complicated one. The drag of such a shape may be

conveniently divided into three parts: pressure, base pressure, and friction. For practical cases, the calculation of the friction drag will likely give the least trouble. However, accuracy in the calculation of the side and base pressures is harder to come by and is especially poor for those shapes which are advantageous for other than aerodynamic reasons (that is, low fineness ratios dictated by savings in structure and weight). For bodies with jets issuing from all or part of the base, the minimum-drag problem is even further complicated, and this phase of the problem will not be dealt with in this report. (See ref. 1.) This report then presents the results of an experiment to determine the zero-lift drag effects of afterbody fineness ratio and shape for a range of designs considered of practical interest, and the results are strictly applicable only to bodies having no jet issuing from the base.

The models were launched from the Langley helium gun at the testing station at Wallops Island, Va., and data were obtained for Mach numbers from 0.8 to 1.3 and for Reynolds numbers (based on body length) of about 10×10^6.

SYMBOLS

x	body station measured from maximum diameter
r	body radius at station x
l	length of body section (either nose or afterbody)
R_m	maximum radius of body
R_b	radius of base of model
ϵ	conical afterbody angle, deg
d	maximum diameter
l/d	fineness ratio
M	Mach number
C_D	drag coefficient, $\dfrac{\text{Drag}}{\text{Dynamic pressure} \times \pi R_m^2}$

MODELS AND DATA REDUCTION

The geometry and dimensions of the afterbody test models are presented in figure 1 and photographs in figure 2. The short and medium-length bodies were constructed entirely of metal, while the long bodies had wooden forebodies and wooden and metal afterbodies. All the fins were metal and the ratio of their exposed area to the frontal area of the body was 5.505 for all models. The trailing edges of all fins intersected the body center line at about the 87-percent body station.

The nose for all models was a parabolic arc given by the following equation:

$$r/R_m = 1 - (x/l)^2$$

Four parabolic and two conical afterbodies were tested for each of two afterbody fineness ratios (l/d = 1.78 and 5.00) while only four parabolic afterbodies were tested of l/d = 3.50.

The parabolic meridians are defined by the following equation:

$$r/R_m = 1 - \left(1 - R_b/R_m\right)(x/l)^2$$

The meridians of the conical afterbodies were constructed by connecting their base diameters and maximum diameters with a straight taper. The resulting afterbody angles are shown in the following table:

l/d	R_b/R_m	ϵ, deg
1.78	0.438	9.0
	.700	4.8
5.00	0.438	3.2
	.700	1.7

The models were launched from the Langley helium gun (described in ref. 2). Their velocities were measured by Doppler radar and corrected to true airspeeds by vector addition of the wind velocity. The Doppler

velocity-time variation was differentiated to give the model acceleration as a function of time. Integration of this velocity gave a flight path. The flight-path angles were used to eliminate the gravity component from the total acceleration and the drag force on the model was then calculated from this corrected acceleration and the model weight. The NACA standard atmosphere tables, corrected to the ground conditions at firing, were used together with the flight path to obtain the variation of density and velocity of sound with time, and these variations were used to calculate the drag coefficients from the drag forces obtained as above.

The actual temperature variations with altitude may be different from the standard tables by enough to give mean errors in the velocity of sound of the order of ±10 feet per second. This corresponds to errors of ±0.005 in C_D and ±0.01 in M. Since this change in temperature is a rather erratic function of altitude at these low altitudes, these possible errors in C_D and M will vary with Mach number for any particular model. The models were fired in the groups shown in the table below and, since the elapsed time between the first and last model of any group was never more than two hours the temperature variation with altitude may be assumed to be a constant for the models of that group. Thus, comparisons between the models of any one group could be more accurate than the figures quoted above.

$l/d = 1.78$

Firing group I, $R_b/R_m = 1, 0.7, 0.438$, and 0 parabolic

Firing group II, $R_b/R_m = 0.7$ and 0.438 conical

$l/d = 3.5$

Firing group III, $R_b/R_m = 1, 0.7, 0.438$, and 0 parabolic

$l/d = 5.00$

Firing group IV, $R_b/R_m = 0.7, 0.438$, 0 parabolic, and 0.7 conical

Firing group I, $R_b/R_m = 0.438$ conical

Firing group V, $R_b/R_m = 1.0$

Experience with previous models (for which the actual temperature variations were known) has indicated that the accuracy in Mach number is indeed better, being of the order of ±0.005M. In C_D, however, the order of the error due to all causes other than temperature variations is ±0.008. For one model (conical, $R_b/R_m = 0.7$, $l/d = 1.78$) the uncertainty in C_D above $M = 1.05$ is ±0.015 due to noise in the radar signal.

Data were obtained for a Mach number range of 0.8 to 1.30 and for Reynolds numbers (based on body length) between 6×10^6 and 8.5×10^6, 7.2×10^6 and 10.1×10^6, and 8.2×10^6 and 11.6×10^6 for the short, medium, and long bodies, respectively.

RESULTS AND DISCUSSION

Total Drag

Total drag coefficients for all the parabolic models are presented as a function of Mach number in figure 3. The variation in drag with R_b/R_m between models of the same fineness ratio at subsonic speeds is due mainly to the differences in base pressure drag. At supersonic speeds this variation is complicated by the addition of wave drag which is a function of both R_b/R_m and the shape of the surfaces.

An effect of afterbody shape is shown in figure 4 which presents the total drag coefficients for all the models with conical afterbodies together with the corresponding parabolic models. The difference is large only for the short afterbodies for which the conical boattails showed an appreciably lower drag at supersonic speeds for both base ratios tested. This effect of shape is shown qualitatively by linearized theory (ref. 3) as well as by the method of characteristics. (See discussion of fig. 6.)

Drag Breakdown

Since this report is concerned mainly with afterbody drag, all components not due directly to the afterbody itself are classified as "tare drag." The tare drags are shown in figure 5 by the shaded areas. The values of three of these drags have been estimated as follows:

(1) Nose pressure drag: method of characteristics, reference 4

(2) Nose friction drag: Van Driest (turbulent), reference 5

(3) Fin drag: measured on a cylindrical rocket model, reference 6

The accuracy of the sum of these three drag coefficients plus the afterbody friction drag is probably within the accuracy of the data since the difference between this sum and the measured drag for the bodies with the $R_b/R_m = 1$ is in all cases the same and is of the order of the base pressure for cylindrical bodies presented in reference 7.

For the models having convergent afterbodies, there are two tare components which cannot be calculated as accurately as those already discussed, but whose magnitudes can be estimated. One, the effect of the nose on the afterbody pressures, has been calculated by linear theory (ref. 3) for the parabolic afterbodies only; it seems reasonable that the interference on the conical afterbodies would not be appreciably different.

The other tare component which should be subtracted from the data is the drag due to the mutual interference of the fin and afterbodies. This is a difficult quantity to determine, and a detailed account of efforts to date is presented in the appendix. For the purposes of this report, however, it seems reasonable to assume that because of the low thickness of the fins ($t/c = 0.0278$) the interference drag is small and that its effect on comparisons between models will be negligible.

The unshaded area under the drag curves of figure 5 represents the components of drag due directly to the afterbody. The friction drag was computed by the method of Van Driest.

The base-drag estimations indicated by the areas so marked in figure 5 were made by simply fairing a line through three points, whose base drags were obtained as follows:

(1) $R_b/R_m = 0.438$: Experimental values from similar rocket models, reference 8

(2) $R_b/R_m = 0.7$: Base drag calculated using value of base pressure midway between the experimental values at $R_b/R_m = 0.438$ and the present test results at $R_b/R_m = 1$

(3) $R_b/R_m = 1$: Present test results

The use of rocket-model data obtained at higher Reynolds numbers (approximately 30×10^6 as compared with 10×10^6 of the present tests) is justified since it is reasonably certain that there is turbulent flow at the base of all the bodies at both Reynolds numbers. This is true of the test models even though they appear to be in a critical range of Reynolds numbers, since the presence of the fins makes transition fairly certain.

Since the method used above is quite arbitrary for all values of R_b/R_m other than 0.438, calculations of the base pressures for all the afterbodies with $l/d = 1.78$ or 5.00 were made by the method of reference 7. Values for the Mach number and pressure coefficient immediately

ahead of the base required in these calculations were obtained by the method of characteristics. The values of base drag obtained in this way for the afterbodies with $R_b/R_m = 0.438$ and $l/d = 1.78$ or 5.00 were considerably lower than the measured values and were in fact negative for the afterbodies with $l/d = 1.78$. The base drag calculated for the parabolic afterbody with $R_b/R_m = 0.7$ and $l/d = 1.78$ was of the order of the experimental values for the afterbody with $R_b/R_m = 0.438$ and thus appeared to be much too low. The calculation for the parabolic afterbody of $R_b/R_m = 0.7$ and $l/d = 5.00$ resulted in a value so close to that estimated in the rough manner described above that the calculated value was substituted in figure 5 for the previously estimated value. Thus the calculations by the method of reference 7 were not used (with the one exception noted previously) and the estimations of the base drags shown in figure 5 are somewhat qualitative. This should be kept in mind when assessing the results shown in figure 6.

Comparison of Experimental and Theoretical Afterbody Pressure Drag

The differences between the total measured drags and the sum of the tare, afterbody friction, and base drags can be called afterbody pressure drags and are shown as the experimental afterbody drags in figure 6. These pressure drags have two components. (The afterbody pressures are also affected by the nose shape; however, this drag component has been subtracted out as part of the tare drag.) The main part is the drag due to the pressures on the afterbody caused by the afterbody shape alone. The other component is that due to the pressures caused by the field of influence of the fins and, as mentioned previously, this drag is thought to be small (see appendix). The theoretical calculations shown were made by the method of characteristics and by the linear method of reference 3. The agreement between the two theoretical methods for afterbodies of $l/d = 1.78$ and their comparative disagreement for those of $l/d = 5.00$ is somewhat surprising. Both theoretical calculations and experimental results indicate that the difference in drag between the conical and parabolic afterbodies is due mainly to the difference in afterbody pressure drag.

In general, the accuracy of the linear calculations is good. The variation of the linear pressure drag with R_b/R_m is accurate enough so that (as may be inferred from figs. 5 and 6) it may be used to predict afterbody geometry for minimum drag at any of the values of l/d used. Significant differences occur between the theoretical and experimental results for the bodies with $l/d = 1.78$ and $R_b/R_m \leq 0.438$.

These differences are probably mainly the result of separated flow on these sharply converging afterbodies but may be partly due to fin interference (see appendix) and to the inadequacies and inaccuracies of the theories. (This is true even for the method of characteristics since the size of the net used for constant accuracy becomes rapidly smaller as the body surface approaches its center line).

Afterbody Design Criteria

The designer is anxious to ascertain the total drag of the afterbody. This drag consists of pressure, base pressure, and friction drag. These total afterbody drags are presented for $M = 1.2$ in figure 7 and were obtained by subtracting the tare drags from the measured total drags. It is immediately apparent from this comparison that, for values of R_b/R_m greater than 0.7, it is useless to extend the length of the afterbody to obtain lower drag; below a ratio of 0.7, of course, large reductions can be effected by such lengthening. Also of interest is the fact that, for the longest afterbody, the range of values of R_b/R_m for near-minimum drag is much larger $(R_b/R_m = 0 \text{ to } 0.4)$ than for the shortest afterbodies $(R_b/R_m = 0.6 \text{ to } 0.8)$.

The effect of the friction component is best shown by the data presented in figure 8 for a Mach number of 1.4. These data were obtained from the rocket models of reference 8 which were fin-stabilized configurations having parabolic meridians and R_b/R_m equal to 0.438 and were of varying fineness ratio and position of maximum diameter. The afterbody drag was obtained by subtracting the component drags determined as follows:

(1) Nose pressure drag: Von Kármán and Moore, reference 9

(2) Friction drag: Van Driest, reference 5

(3) Fin drag: measured on cylindrical rocket models, reference 6

(4) Base drag: measured for all models, reference 8

This breakdown is only qualitatively correct since the models had noses of widely different fineness ratio - in some cases quite short - and thus their drag estimations are subject to fairly large error. In addition, the varying effects of the different nose lengths on the drag of the afterbody were not accounted for at all. With qualifications then, the effect on base drag due to increasing l/d is small, the pressure drag rapidly decreases and the friction drag increases as l/d is

increased and these opposing trends cause the minimum-drag configuration to be that with an l/d of about 6.

Ideally, the designer would like a chart of minimum-drag configurations for all values of R_b/R_m and l/d together with the amount of drag saved by use of such configurations. Though admittedly the data are meager, such charts are presented in figures 9 and 10. The three points shown for minimum-drag configurations were taken from figure 7 for the parabolic afterbodies; however, they are equally valid for the conical afterbodies. The fact that a straight line connects these three points with that of the body with a square base and $l/d = 0$ seems to be significant, since such a line represents afterbodies of constant base angle for either conical or parabolic afterbodies. (The tangent of the parabolic base angle is always exactly twice that of the inscribed conical afterbody). The present results indicate that afterbodies of about 4.5° conical angle or 9.0° parabolic base angle will give the minimum drag for any value of l/d chosen (for $l/d < 6$, of course). This line intersects the line $R_b/R_m = 0$ at $l/d = 6$ which again indicates that an afterbody of fineness ratio 6 is about the optimum. (See fig. 8.) As mentioned in the discussion of figure 7, the dependence of the drag for near-minimum configurations upon R_b/R_m is quite a bit less for the afterbodies with higher l/d. This is shown in more useful form by the shaded area surrounding the minimum-drag-configuration line. This area indicates all configurations which for a given l/d have drags which are within approximately 10 percent of the minimum drag for that l/d, and corresponds to conical base angles between 6.5° and 3.5°. The range of optimum conical angles indicated (3.5° to 6.5°) is of the same order (5° to 7°) as that used for quite some time by ballisticians for the drag reduction of bullets. There is no reference for this remark, but there is one early paper (ref. 10) which analyzed the conical-afterbody problem using very crude assumptions as to the pressure on the afterbody and base, and which arrived at a similar answer (that is, optimum angles of about 5° for the moderate supersonic Mach numbers). The main disagreement with the present tests was the prediction that the optimum angle decreased rapidly for values of l/d greater than 2.

An indication of how much the drag may be reduced by proper design results when the data of figure 7 are divided by the cylindrical-base drag and presented as functions of l/d (again this is for parabolic afterbodies but applies qualitatively to conical as well). It is apparent from this plot (fig. 10) together with the previous plot (fig. 9) that it is possible to reduce the drag to 30 percent or 40 percent of the square-base drag if the designer can afford an afterbody of fineness ratio of 5 or 6 and R_b/R_m of 0.4 or less. The rocket-model data (fig. 8) have been plotted on the same figure for comparison and

show the same general trends. Due to the qualitative nature of the data for $M = 1.4$, it is impossible to state anything about the effect of Mach number on either the shape of the optimum afterbodies or the magnitudes of the possible drag reductions.

CONCLUSIONS

Free-flight measurements at Mach numbers from 0.8 to 1.3 of the zero-lift drag of a series of fin-stabilized bodies differing only in afterbody shape and fineness ratio indicate the following conclusions. These conclusions apply only to models without a jet exiting from the base and only at moderate supersonic Mach numbers.

1. For the shortest afterbodies ($l/d = 1.78$, where l is length and d is maximum diameter), the boattails with conical meridians showed appreciably lower drag than those of parabolic section. The drags for the two shapes were essentially the same for the afterbodies of $l/d = 5$. Both of these conclusions are predicted qualitatively by linearized theory and by the method of characteristics.

2. Linear theory was adequate to determine the minimum-drag afterbody geometry for the shape parameters tested and gave a fair estimate of the drag for all afterbodies of $l/d = 3.5$ or 5.00.

From the test results, the following would appear to be useful design criteria:

1. A conical boattail of angle about 4.5° will give the minimum drag for any value of l/d less than 6. For configurations with drags within 10 percent of the minimum, the conical boattail angle may vary between 3.5° and 6.5°.

2. The minimum-drag afterbody has a fineness ratio of about 6 and its drag is approximately 30 percent to 40 percent of the drag for a square-based body of $l/d = 0$.

Langley Aeronautical Laboratory,
National Advisory Committee for Aeronautics,
Langley Field, Va., August 12, 1953.

APPENDIX

EFFECT OF FINS ON AFTERBODY PRESSURE DRAG

Because of the low thickness ratio of the fins their effects on the pressure drag of the afterbodies presented in this report has been assumed small. Several attempts have been made to check this assumption theoretically and experimentally.

The mutual-interference effects of the fins and afterbody have been estimated theoretically by Mr. R. L Nelson of the Langley Laboratory by use of the premise that the pressure drag of the fin-afterbody combination is equal to that of a body of revolution of equivalent cross-sectional area distribution. (For experimental confirmation of this assumption see ref. 11.) These equivalent-area distributions have been calculated for the afterbodies with $l/d = 1.78$ and 5.00 and are shown in figure 11. In order to simplify the calculations, the fin-area distributions were approximated by parabolic distributions and the actual fin and body constants (area ratios, spans, location of fins on the afterbody) were generalized as shown in figure 12. The simplification causing the greatest differences between the real and the mathematical models was the fixing of the fin tip at the base of the model, and this should not affect the results appreciably. The interference drags were calculated with the linear equations of reference 3 and these drags are presented in figure 12. The results indicate that with the exception of the afterbodies of $l/d = 1.78$ the interference drags were small and of the order of the test accuracy. The results, however, predicted a rather startlingly large negative interference for the afterbodies of $l/d = 1.78$.

Since these interference drags were so large, an attempt was made to substantiate the calculations experimentally and the configuration with the largest predicted interference was chosen. The two models tested are shown at the top of figure 13. The afterbody and fins of model 1 are identical to those of the model with $l/d = 1.78$ and $R_b/R_m = 0$, the drag of which is presented in figure 3. The body of model 2 is identical to that of model 1 and the fins are located on the cylindrical center section far enough forward so that the Mach lines from their tips do not intersect the convergent afterbody surface until $M > 1.2$. The comparison of the drag coefficients of models 1 and 2 does not show the expected favorable interference, the moving of the fin influence off the afterbody causing in fact a lower supersonic drag as well as a lower drag rise. The changes in fin position had a large effect on the subsonic drag also. This effect may be due to changes in boundary-layer transition, and to varying amounts of separation over the afterbody. (The Reynolds numbers

based on body length varied from 7.8×10^6 at $M = 0.8$ to 12.5×10^6 at $M = 1.25$). Since both the transition and the separation phenomena may have been varying during the passage through the supersonic range they may have changed the effects of fin interference entirely. Thus while the test models leave the question of the accuracy of the linear predictions still open they do indicate that the effect of the fins will be substantially different than that calculated for sharply convergent afterbodies. In this light, the absolute values of the afterbody pressure drags for the afterbodies with $l/d = 1.78$ and $R_b/R_m = 0$ or 0.438 may be more suspect and more a function of the fins than the drags of the remaining afterbodies in these tests.

REFERENCES

1. Cortright, Edgar M., Jr., and Schroeder, Albert H.: Investigation at a Mach Number 1.91 of Side and Base Pressure Distributions Over Conical Boattails Without and With Jet Flow Issuing From Base. NACA RM E51F26, 1951.

2. Mitcham, Grady L., and Blanchard, William S., Jr.: Low-Lift Drag and Stability Data From Rocket Models of a Modified-Delta-Wing Airplane With and Without External Stores at Mach Numbers From 0.8 to 1.36. NACA RM L53A27, 1953.

3. Fraenkel, L. E.: The Theoretical Wave Drag of Some Bodies of Revolution. Rep. No. Aero 2420, British R.A.E., May 1951.

4. Ferri, Antonio: Application of the Method of Characteristics to Supersonic Rotational Flow. NACA Rep. 841, 1946. (Supersedes NACA TN 1135.)

5. Van Driest, E. R.: Turbulent Boundary Layer in Compressible Fluids. Jour. Aero. Sci., vol. 18, no. 3, Mar. 1951, pp. 145-160, 216.

6. Stoney, William E., Jr.: Pressure Distributions at Mach Numbers From 0.6 to 1.9 Measured in Free Flight on a Parabolic Body of Revolution With Sharply Convergent Afterbody. NACA RM L51L03, 1952.

7. Love, Eugene S.: The Base Pressure at Supersonic Speeds on Two-Dimensional Airfoils and Bodies of Revolution (With and Without Fins) Having Turbulent Boundary Layers. NACA RM L53C02, 1953.

8. Katz, Ellis R., and Stoney, William E., Jr.: Base Pressures Measured on Several Parabolic-Arc Bodies of Revolution in Free Flight at Mach Numbers From 0.8 to 1.4 and at Large Reynolds Numbers. NACA RM L51F29, 1951.

9. Von Kármán, Theodor, and Moore, Norton B.: Resistance of Slender Bodies Moving With Supersonic Velocities With Special Reference to Projectiles. Trans. A.S.M.E., vol. 54, no. 23, Dec. 15, 1932, pp. 303-310.

10. Boreli, F.: Pressure Distribution Measurements on Models of Projectiles. Rep. No. F.R. 340, Douglas Aircraft Co., Inc., Apr. 4, 1947. (Available from CADO as ATI 2457.) (Translation of UM Nr. 6057, Aerodynamisches Institut T. H. Aachen, Mar. 6, 1945.)

11. Whitcomb, Richard T.: A Study of the Zero-Lift Drag-Rise Characteristics of Wing-Body Combinations Near the Speed of Sound. NACA RM L52H08, 1952.

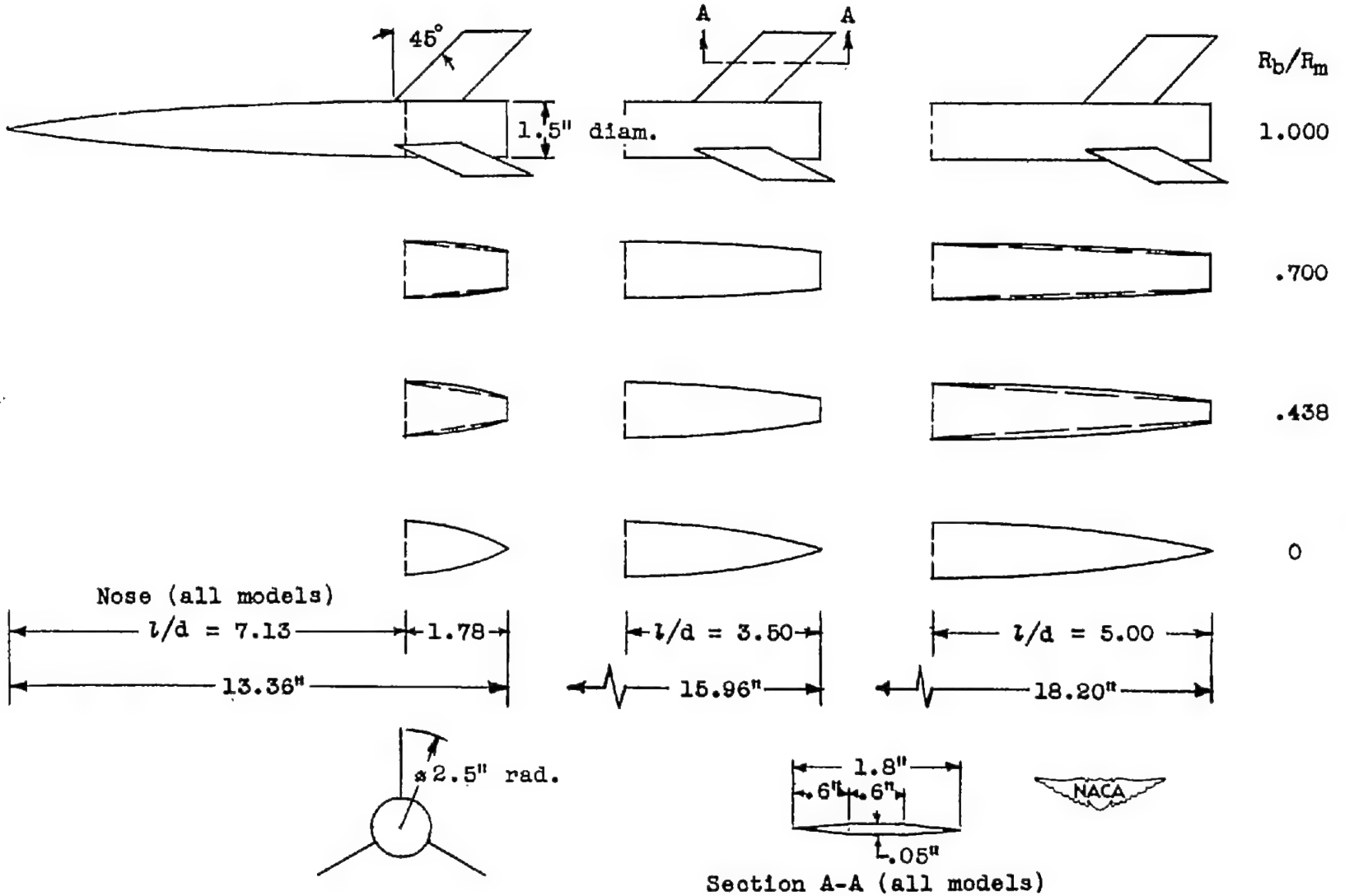

Figure 1.- Test configurations.

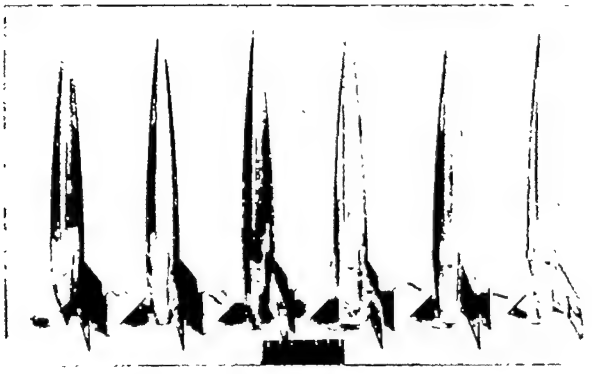

L-75338

(a) Afterbodies of $l/d = 1.78$.

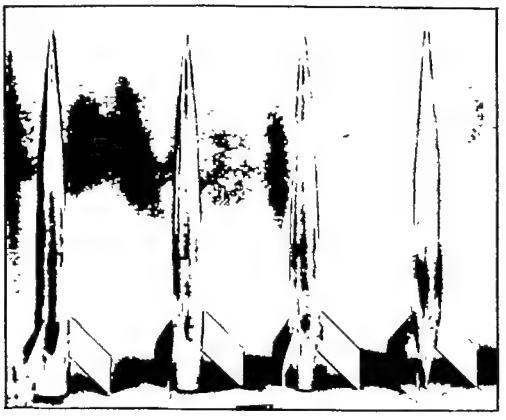

L-79432

(b) Afterbodies of $l/d = 3.50$.

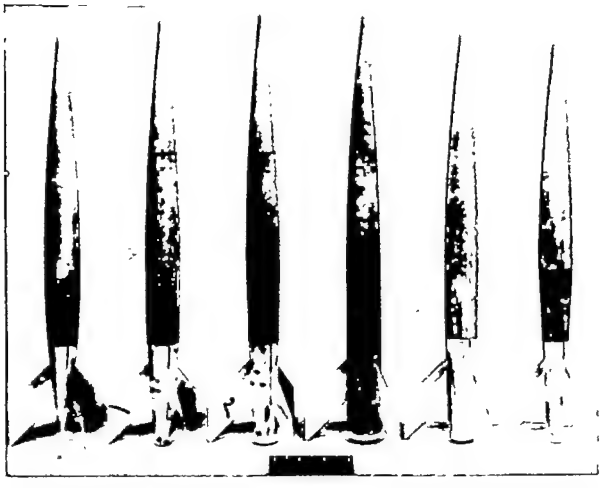

L-75339

(c) Afterbodies of $l/d = 5.00$.

Figure 2.- Model photographs.

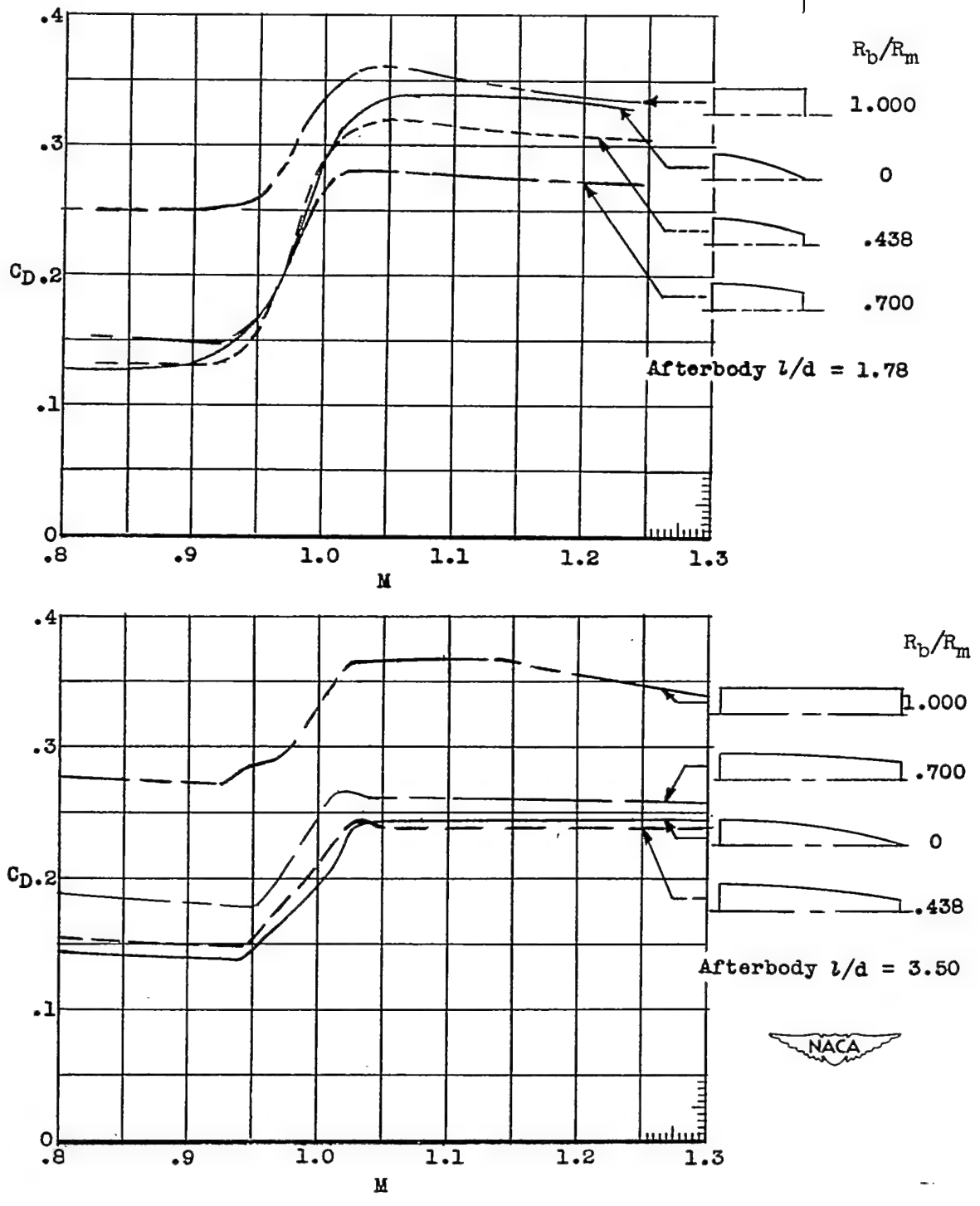

Figure 3.- Total-configuration drag coefficients of parabolic afterbodies.

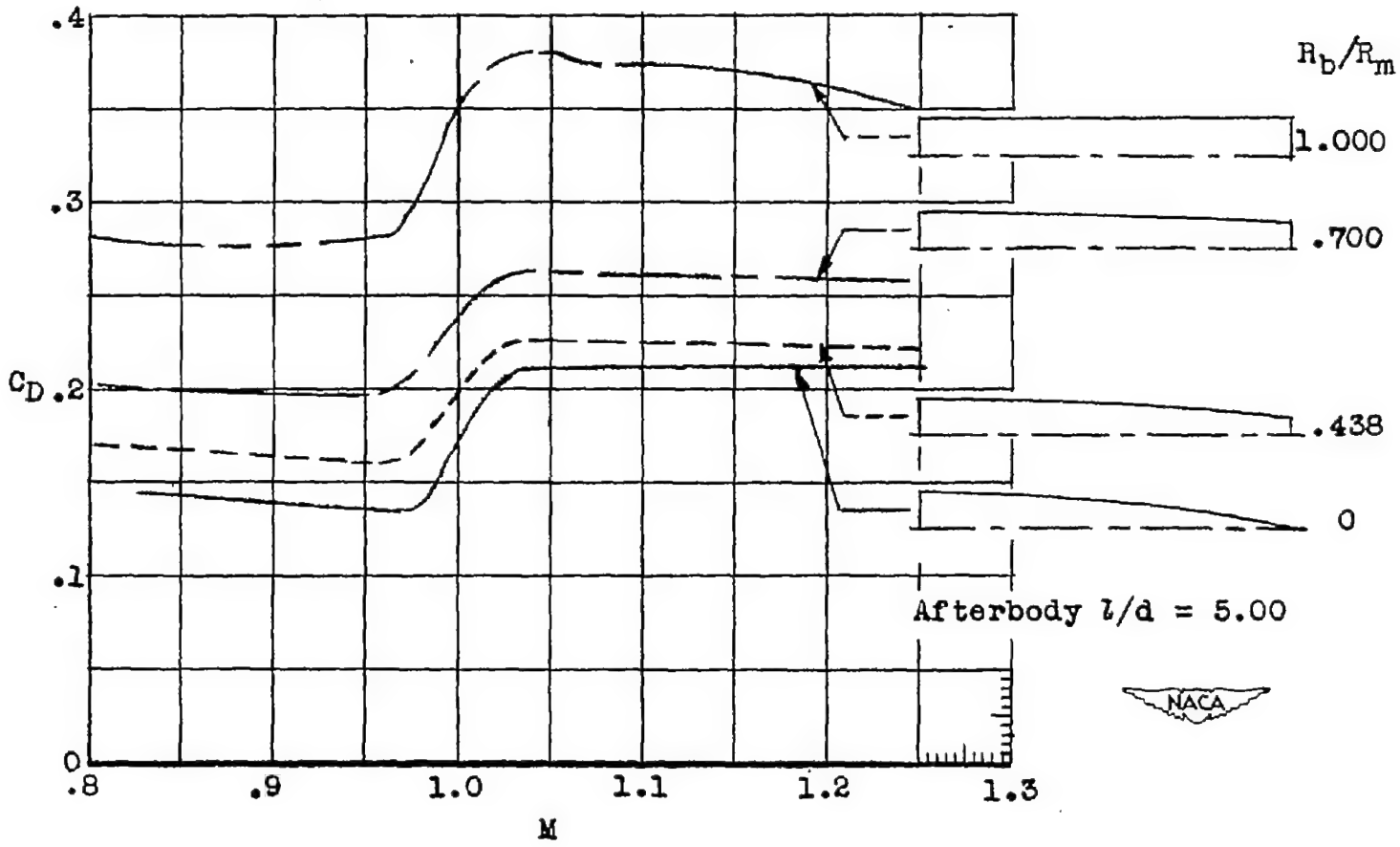

Figure 3.- Concluded.

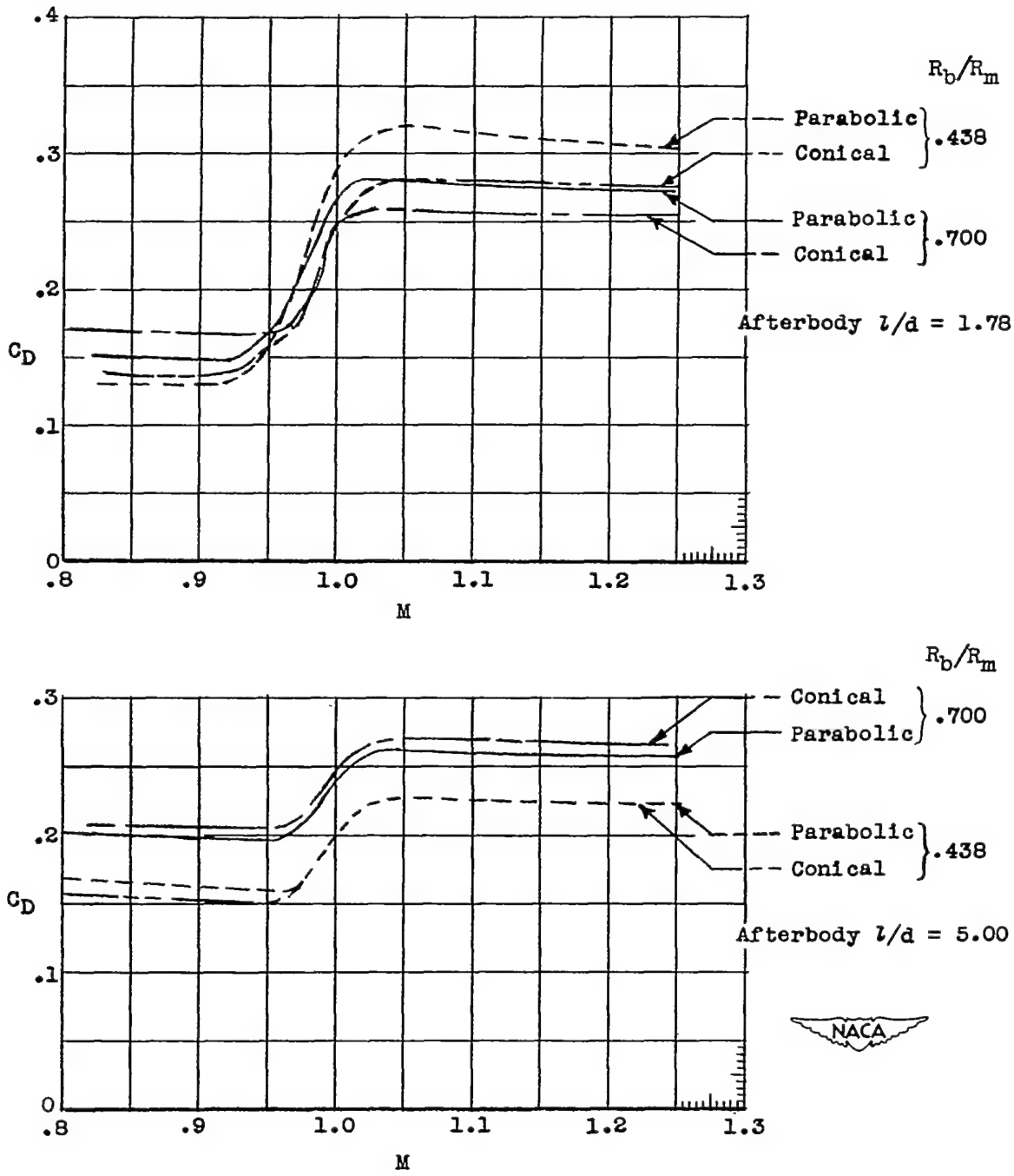

Figure 4.- Comparison of total drag coefficients of parabolic and conical afterbody models.

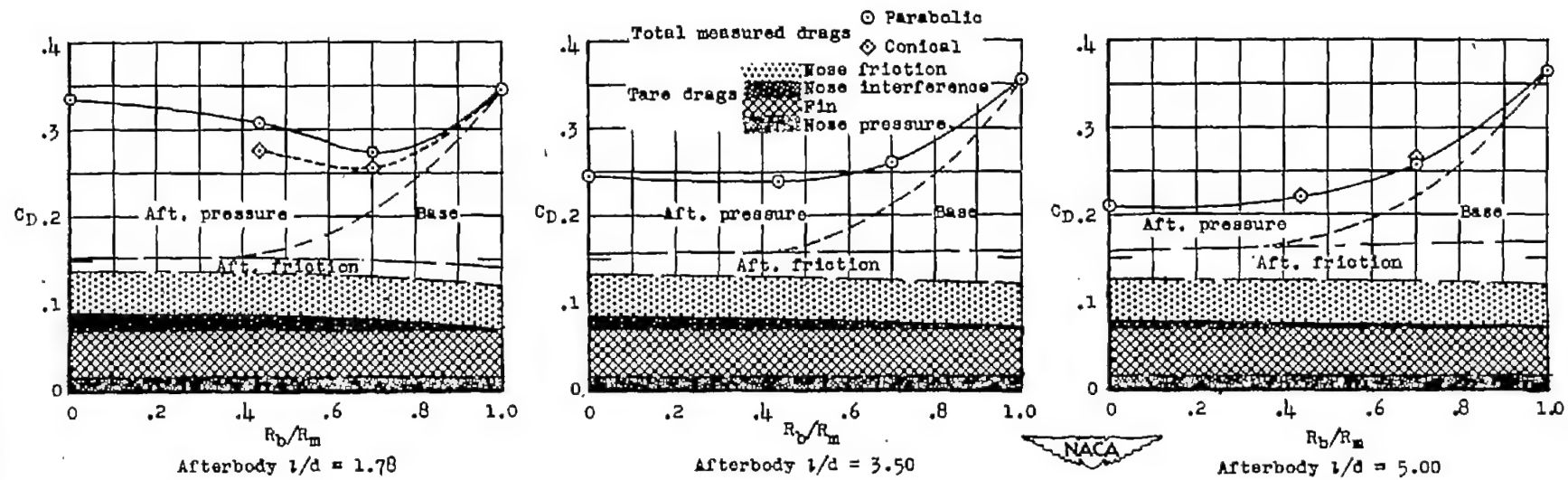

Figure 5.- Drag breakdown at M = 1.2.

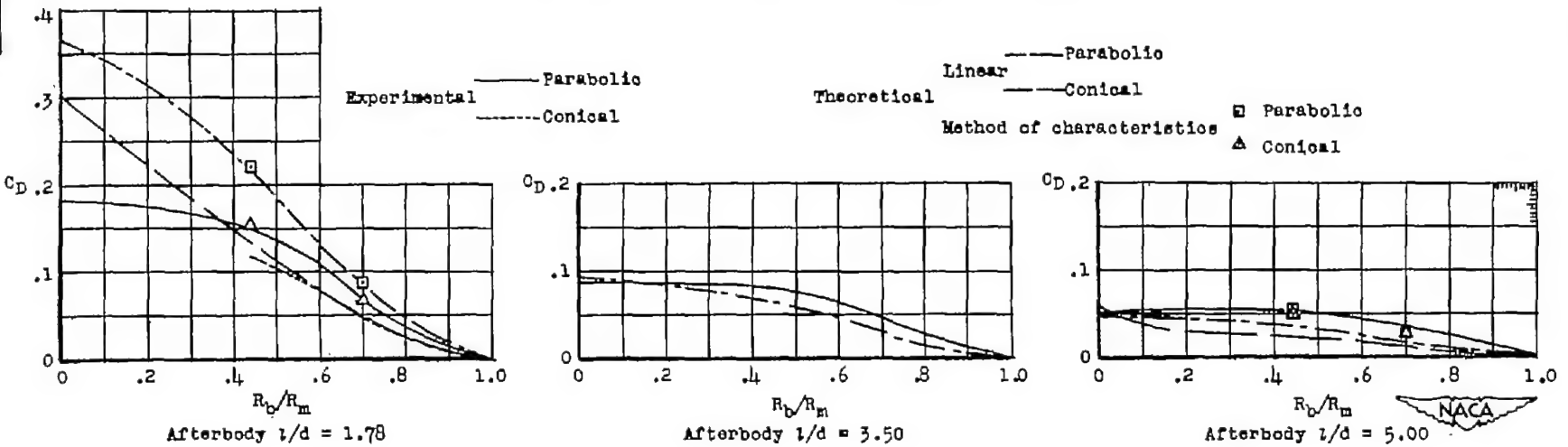

Figure 6.- Comparison of experimental and theoretical afterbody pressure drags at M = 1.2.

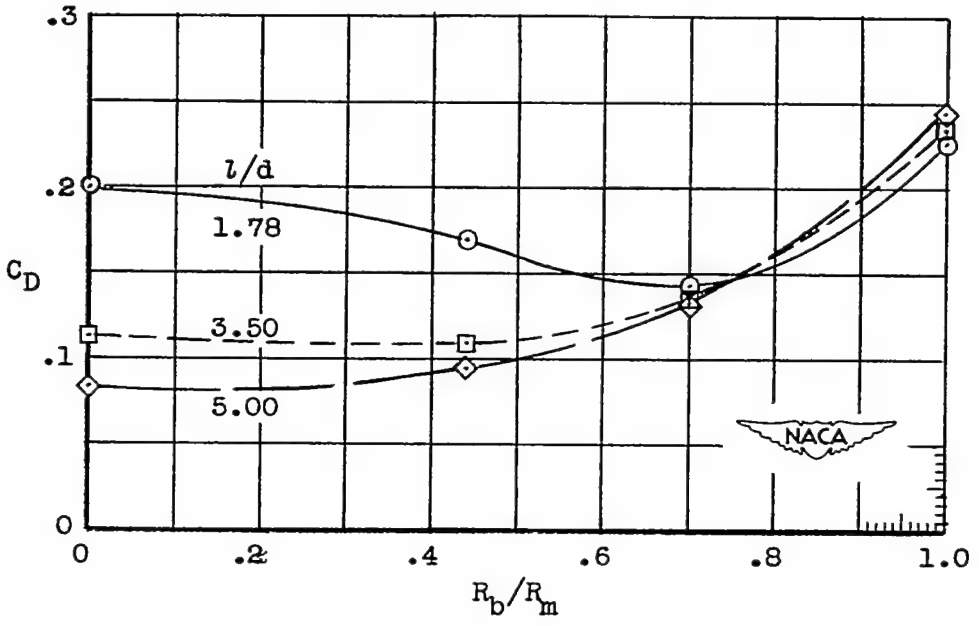

Figure 7.- Total parabolic afterbody drag = Pressure drag + Base drag + Friction drag. M = 1.2.

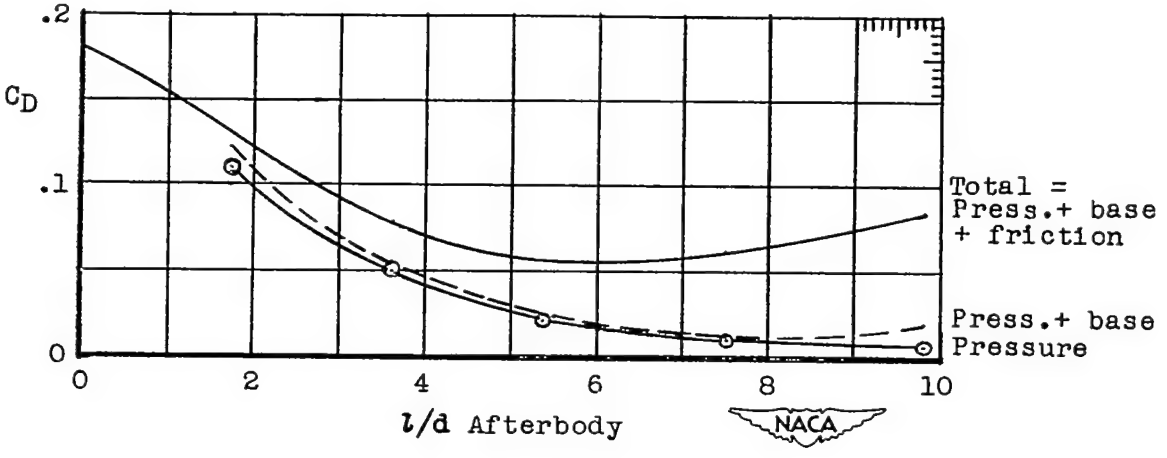

Figure 8.- Qualitative breakdown of afterbody drag for models of reference 8. R_b/R_m = 0.438; M = 1.4.

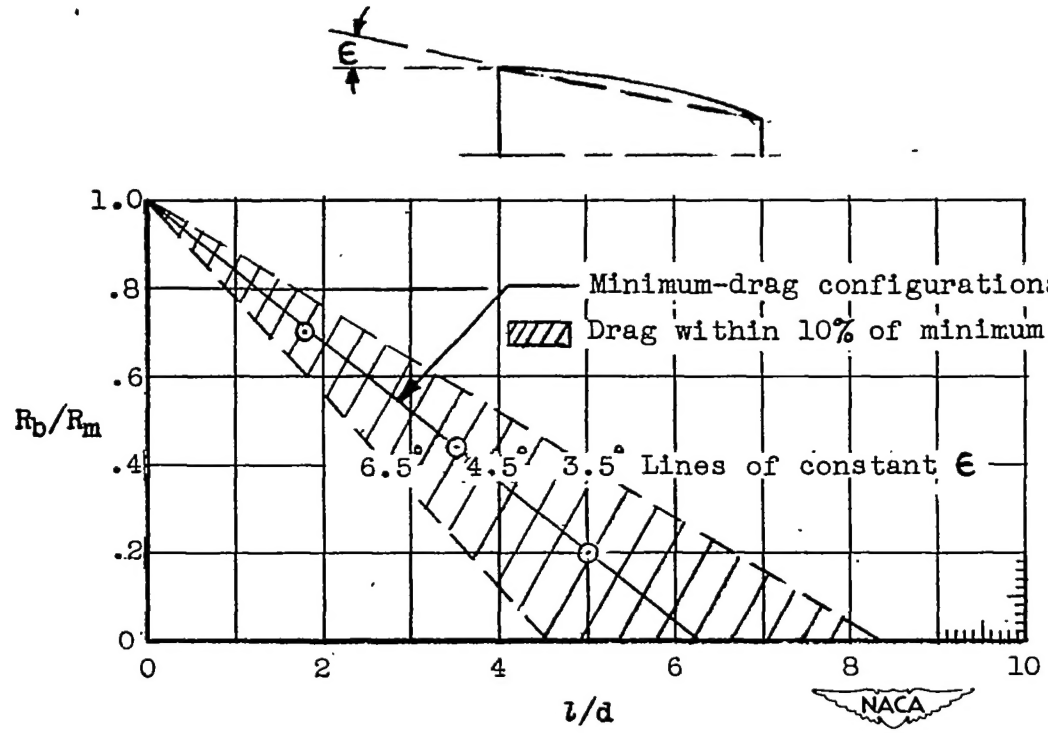

Figure 9.- Minimum-drag configurations at M = 1.2.

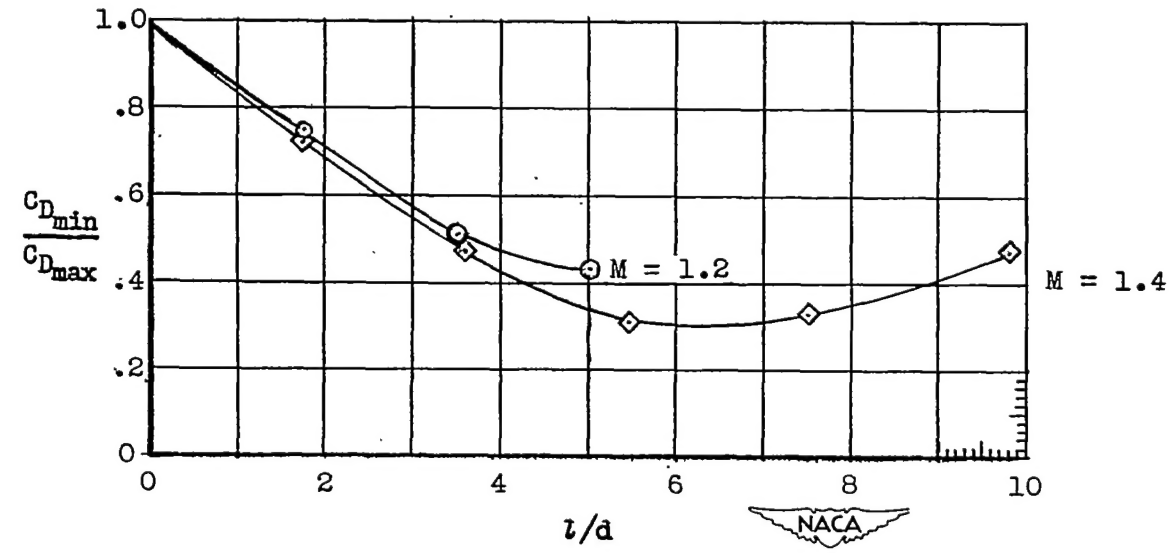

Figure 10.- Ratios of drag of minimum-drag configurations to drag of a cylindrical afterbody of $l/d = 0$ at $M = 1.2$ compared with data of rocket model of $R_b/R_m = 0.438$ at $M = 1.4$.

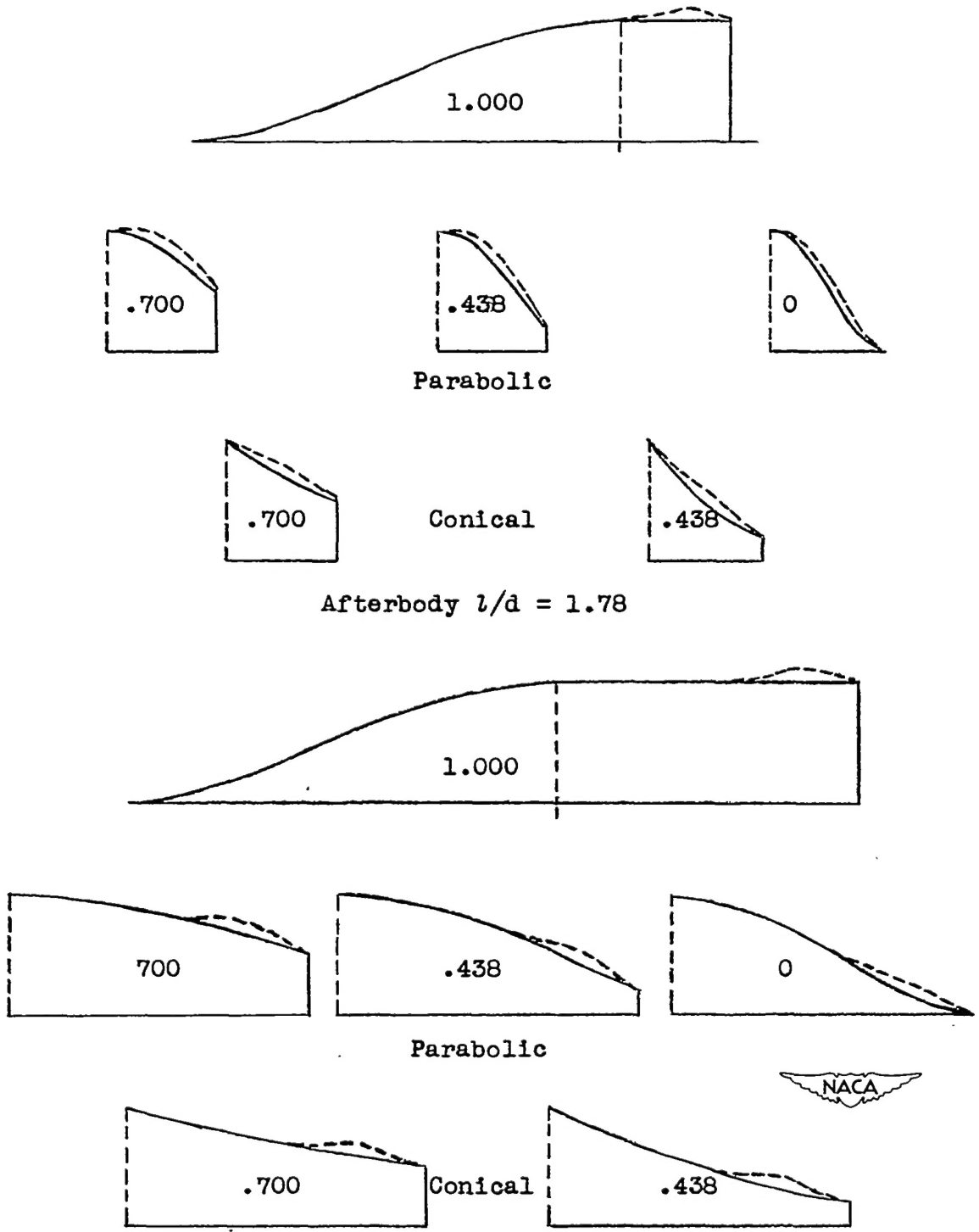

Figure 11.- Longitudinal area distributions.

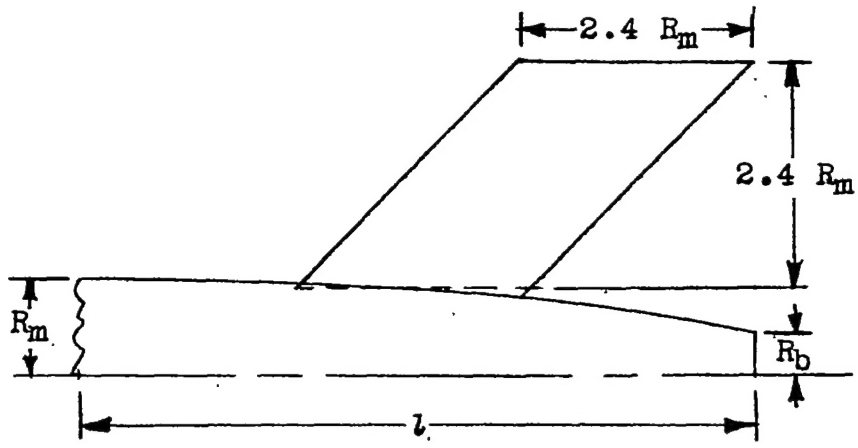

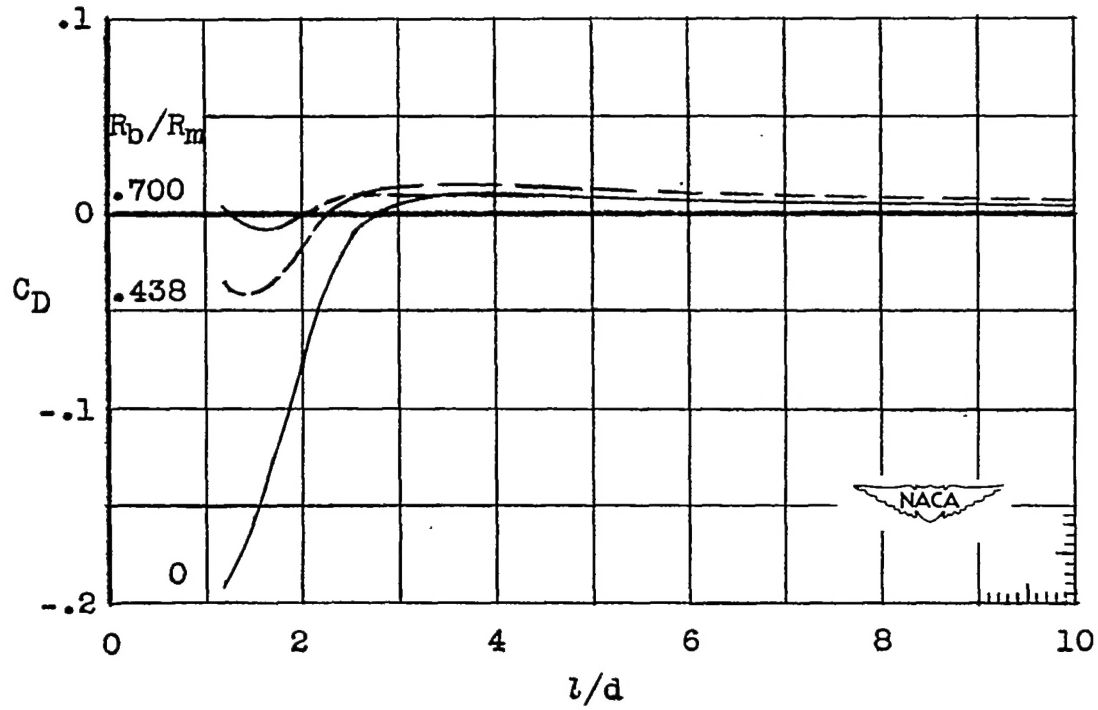

Figure 12.- Theoretical interference drag between fins and parabolic afterbodies.

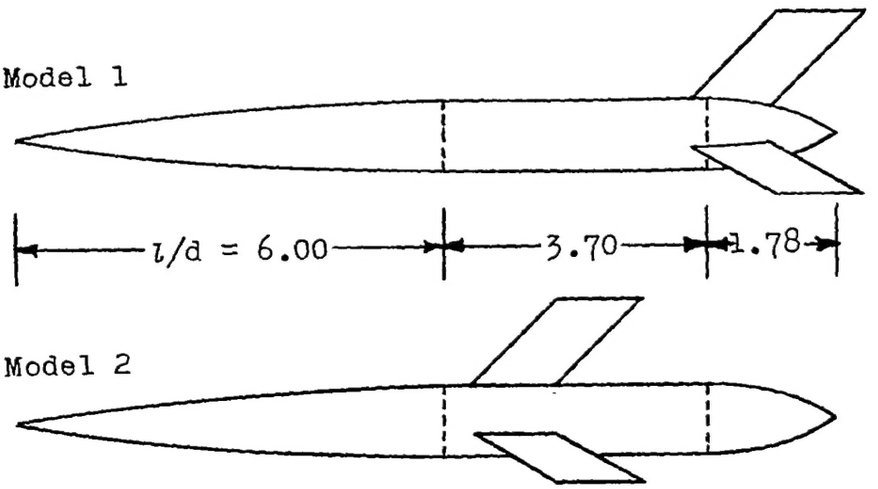

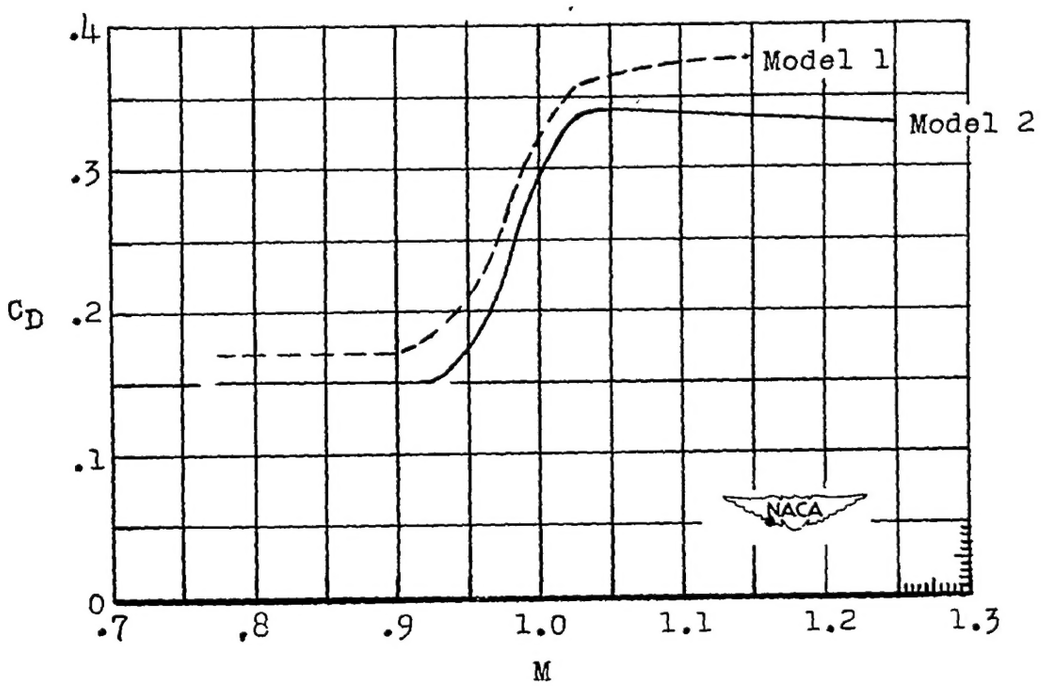

Figure 13.- Drag coefficients of fin-interference test models.

NACA-Langley - 10-1-53 - 325